Dalton Transactions

Near-Infrared C-term MCD Spectroscopy of Octahedral Uranium(V) Complexes

Journal:	*Dalton Transactions*
Manuscript ID	DT-ART-02-2021-000513.R1
Article Type:	Paper
Date Submitted by the Author:	09-Mar-2021
Complete List of Authors:	Curran, Daniel; University of Rochester, Chemistry Ganguly, Gaurab; University at Buffalo - The State University of New York, Chemistry Heit, Yonaton ; University at Buffalo, State University of New York, Chemistry Wolford, Nikki; University of Rochester, Chemistry Minasian, Stefan; Lawrence Berkeley National Laboratory, Chemical Sciences Division Loble, Matthias; Los Alamos Nation Laboratory, Chemistry Division Cary, Samantha; Los Alamos Nation Laboratory, Chemistry Division Kozimor, Stosh; Los Alamos Nation Laboratory, Chemistry Division Autschbach, Jochen; University at Buffalo, State University of New York, Chemistry Neidig, Michael; University of Rochester, Chemistry

ARTICLE

Near-Infrared C-term MCD Spectroscopy of Octahedral Uranium(V) Complexes

Received 00th January 20xx,
Accepted 00th January 20xx

DOI: 10.1039/x0xx00000x

Daniel J. Curran,[a†] Gaurab Ganguly,[b†] Yonaton N. Heit,[b] Nikki J. Wolford,[a] Stefan G. Minasian,[c] Matthias W. Löble,[d] Samantha K. Cary,[d] Stosh A. Kozimor,[d] Jochen Autschbach[b]* and Michael L. Neidig[a]*

C-term magnetic circular dichroism (MCD) spectroscopy is a powerful method for probing d—d and f—f transitions in paramagnetic transition metal and heavy metal complexes. However, this technique remains underdeveloped both experimentally and theoretically for studies of U(V) complexes of O_h symmetry, which have been of longstanding interest for probing electronic structure, bonding, and covalency in 5f systems. In this study, C-term NIR MCD of the Laporte forbidden f—f transitions of $[UCl_6]^-$ and $[UF_6]^-$ are reported, demonstrating the significant fine structure resolution possible with this technique including for the low energy $\Gamma_7 \rightarrow \Gamma_8$ transitions in $[UF_6]^-$. The experimental NIR MCD studies were further extended to $[U(OC_6F_5)_6]^-$, $[U(CH_2SiMe_3)_6]^-$, and $[U(NC(^tBu)(Ph))_6]^-$ to evaluate the effects of ligand-type on the f—f MCD fine features. Theoretical calculations were conducted to calculate the Laporte forbidden f—f transitions and their MCD intensity experimentally observed in the NIR spectra of the U(V) hexahalide complexes, via the inclusion of vibronic coupling, to better understand the underlying spectral fine structure features for these complexes. These spectra and simulations provide an important platform for the application of MCD spectroscopy to this widely studied class of U(V) complexes and identify areas for continued theoretical development.

Introduction

Evaluation of electronic structure and bonding in uranium coordination complexes through both spectroscopic and theoretical methods has long been an area of intense research interest, motivated by the need to efficiently handle and separate nuclear waste[1] as well as advancing our understanding of uranium's reactivity towards small molecules.[2-4] To define electronic structure and bonding in uranium chemistry, numerous spectroscopic methods have been employed such as electronic absorbance spectroscopy (EAS),[5-10] X-ray absorption spectroscopy (XAS),[11-21] electronic paramagnetic resonance (EPR) spectroscopy,[21-29] and nuclear magnetic resonance (NMR) spectroscopy.[30-32] Besides, computational studies have been widely employed to interrogate electronic structure in uranium chemistry.[33-47] EAS is the most widely employed of these methods, due to its broad availability and the insight it can provide on f—f transitions in the near-infrared (NIR) region, providing a fingerprint to the oxidation states and ligand environments of uranium coordination complexes. While it is extremely useful to probe energy shifts in f—f transitions as a function of ligand perturbation, this method can suffer from overlapping transitions and vibrational overtone contributions from solvent in the NIR region, resulting in the loss of information-rich fine structure features. While similar challenges exist for NIR EAS studies of transition metal complexes, C-term magnetic circular dichroism (MCD) has been alternatively applied to the study of NIR d—d transitions in paramagnetic complexes, especially to obtain high-resolution insight into electronic structure across systems ranging from bioinorganic chemistry to organometallic catalysis in transition metal chemistry.[48-50] Applying this technique to actinide chemistry, uranium in the case of this study, is important to test theory's ability to treat actinide complexes in addition to better understand the differences and similarities between actinides and their transition metals counterparts.

The intensity of an MCD spectrum is proportional to the sum of three contributions which are designated as the A-, B-, and C-terms as shown in eqn (1).

$$\frac{\Delta\mathcal{E}}{E} \propto \left[\boldsymbol{A}\left(-\frac{\partial f(E)}{\partial E}\right) + \left(\boldsymbol{B} + \frac{\boldsymbol{C}}{k_B T}\right) \boldsymbol{f(E)}\right] \quad (1)$$

Here, $\Delta\mathcal{E}$ is the field-dependent difference between the absorption of left- (lcp) and right-circularly polarized (rcp) light, $E\ (= h\nu)$ is the energy of a photon, $f(E)$ is the absorption bandshape simulated by Gaussian functions, and $\partial f(E)/\partial E$ is its first derivative. While all three of these mechanisms may contribute to the MCD spectrum for a paramagnetic uranium

[a] Department of Chemistry, University of Rochester, Rochester, New York 14627, USA. *Email: neidig@chem.rochester.edu
[b] Department of Chemistry, University at Buffalo, State University of New York, Buffalo, New York 14260, USA. *Email: jochena@buffalo.edu
[c] Chemical Sciences Division, Lawrence Berkeley National Laboratory, Berkeley, CA 94720
[d] Chemistry Division, Los Alamos National Laboratory, Los Alamos, New Mexico, 87544
† Daniel J. Curran and Gaurab Ganguly contributed equally to this work.
Electronic Supplementary Information (ESI) available: [details of any supplementary information available should be included here]. See DOI: 10.1039/x0xx00000x

complex, the C-term is the largest contribution at room temperature already, and it is approximately two orders of magnitude larger than the A- and B-term contributions at cryogenic temperatures, dominating low-temperature measurements of paramagnetic uranium complexes. The C-term mechanism requires a degenerate ground-state (GS) and the presence of an applied magnetic field to remove the degeneracy via the Zeeman effect. This removal of the degeneracy in the GS results in differing intensities in lcp and rcp transitions such that they no longer cancel out, resulting in an absorption band shape as shown in Fig. 1 that is both magnetic field and temperature-dependent.

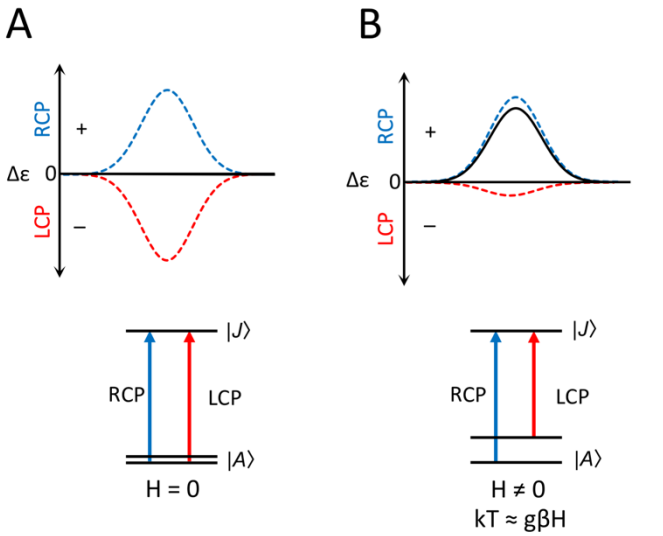

Fig. 1 The C-term MCD mechanism for a J = 1/2 ground state. (A) No C-term MCD intensity is observed in the absence of an applied magnetic field, and (B) C-term intensity in the presence of an applied magnetic field where the two Zeeman split M_J levels are unequally populated, resulting in an MCD transition with an absorption band shape.

The application of NIR C-term MCD in uranium chemistry to evaluate f—f transitions has largely been limited to several recent studies on U(III) and U(IV) complexes.[51-55] Of particular importance is the extension of this method to octahedral (O_h) U(V) (f^1) complexes which have been central to evaluating ligand effects on electronic structure and bonding.[56] However, such an extension is non-trivial due to the role of vibronic coupling to overcome the dipole-forbidden nature of the f—f transitions in complexes containing the center of inversion. Compared to our previous studies on f—f transitions in distorted high coordinate U(III) and U(IV) complexes, this provides a considerable challenge in the computation of the resultant C-term MCD spectra.[54,55]

The present study focuses on the application of C-term MCD spectroscopy to evaluate electronic structure in a series of O_h U(V) complexes, focusing on f—f transitions in the NIR region to directly probe their ligand field (LF) states involving 5f orbitals. Notably, the ground state (GS), denoted by Γ_7, and transition between its excited states (ESs), referenced as Γ_8, $\Gamma_{7'}$, $\Gamma_{8'}$, and Γ_6, were investigated.[9] To our knowledge, this is the first attempt to calculate vibronic MCD of a metal complex from first principles. Experimental and theoretical C-term MCD studies of $[UCl_6]^-$ and $[UF_6]^-$ demonstrate the significant resolution of fine structure features in the NIR region that are achievable as well as the information content and associated challenges in MCD simulations of f—f transitions through the incorporation of vibronic coupling.

Results and Discussion

NIR MCD Spectroscopy of $[UCl_6]^-$

Initial studies focused on evaluating the f—f transitions in $[UCl_6]^-$ in the NIR region using C-term MCD spectroscopy (Fig. 2). The assignments of these transitions are facilitated, due to previously reported NIR electronic absorption studies of this complex.[7] Starting at low energy, the first band observed in the 5 K, 7 T NIR MCD spectrum of $[UCl_6]^-$ is the $\Gamma_7 \rightarrow \Gamma_{7'}$ transition from 6650 to 7150 cm^{-1} (Fig. 2A and 2C). This transition is comprised of three defining features in the fine structure. The first and most intense one is a negative to positive derivative feature with peaks 85 cm^{-1} apart and centered at 6820 cm^{-1}. Within the positive end of the derivative at 6840 cm^{-1}, there is a subtle shoulder on the lower energy side of the peak. There are two features of reduced-intensity adjacent to the derivative shape at slightly higher energy, centered at 6930 and 7100 cm^{-1}, respectively. The 6930 cm^{-1} transition is sharper than the higher energy fine structure feature and has a small tail on its higher energy side.

The next transition, $\Gamma_7 \rightarrow \Gamma_{8'}$, spans 10050 cm^{-1} to 10800 cm^{-1}. This transition is comprised of two noticeable fine structure features, with absorption peaks centered at 10180 cm^{-1} and 10600 cm^{-1}, which are both less intense and broader than the derivative feature observed in the $\Gamma_7 \rightarrow \Gamma_{7'}$ transition. The signal at 10180 cm^{-1} has half the intensity of the signal at 6820 cm^{-1}, while the 10600 cm^{-1} signal is half as intense as the 10180 cm^{-1} feature. From low to high energy, these two fine structure features are 350 and 300 cm^{-1} wide respectively, about seven times wider than either component of the derivative feature. Pure electronic f—f transitions are sharp and intense, providing context to the possible origin of this transition having other contribution mechanisms.

The $\Gamma_7 \rightarrow \Gamma_6$ transition is the highest energy f—f transition observed. This transition is an asymmetrical derivative shape spanning 11400 cm^{-1} to 11875 cm^{-1} with a midpoint at 11750 cm^{-1}. This negative to positive derivative feature is similar to the $\Gamma_7 \rightarrow \Gamma_{8'}$ transition, and relatively weak and broad concerning the $\Gamma_7 \rightarrow \Gamma_{7'}$ transition. The negative fine structure centered at 11575 cm^{-1} is 275 cm^{-1} wide and has about the same intensity as the lower energy signal in the $\Gamma_7 \rightarrow \Gamma_{8'}$ transition. It is slightly asymmetric, with the higher energy side of the peak being rather sharp. From 11675 to 11875 cm^{-1} there is a symmetric positive fine structure that has one-fourth of the intensity of its negative counterpart. Based on the observed fine structure features, the mechanism governing this transition is likely similar to that for the $\Gamma_7 \rightarrow \Gamma_{8'}$ transition.

The high level of resolution of the fine structures of the f—f transitions in the C-term MCD spectrum of $[UCl_6]^-$ compared to typical electronic absorption studies in the NIR region as described above is immediately apparent, demonstrating the

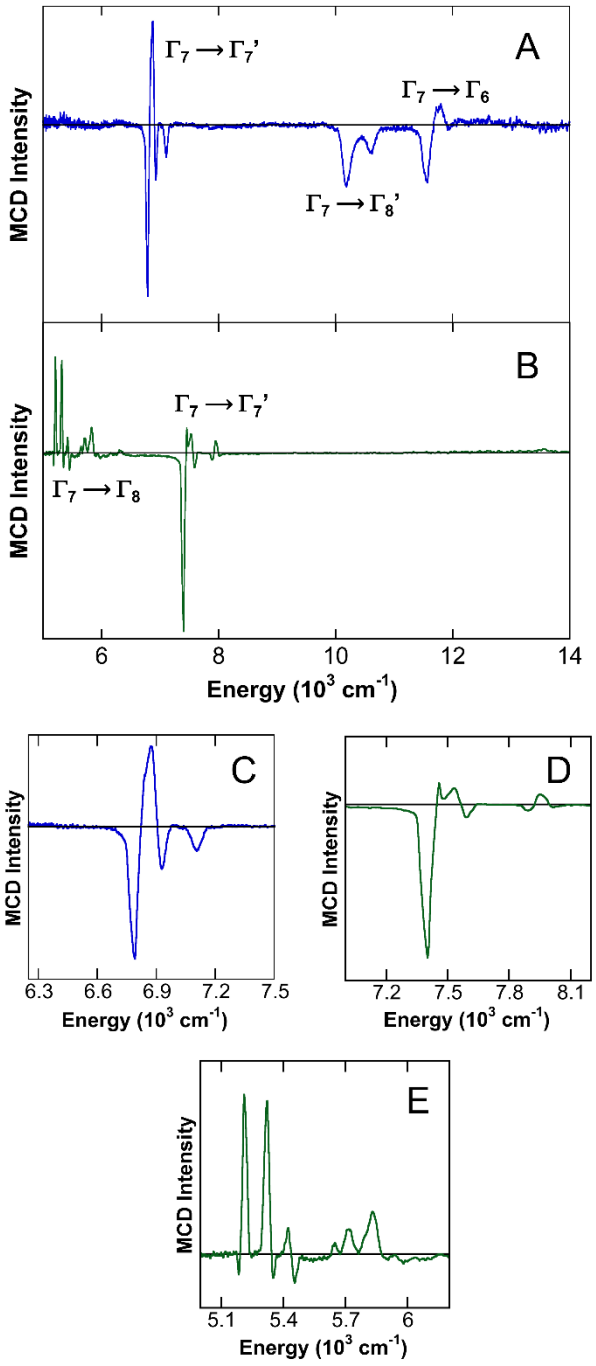

Fig. 2 The 5 K, 7 T NIR MCD spectrum of (A) $[UCl_6]^-$. and (B) $[UF_6]^-$. Enlarged views of the $\Gamma_7 \rightarrow \Gamma_7'$ transitions for (C) $[UCl_6]^-$ and (D) $[UF_6]^-$ and (E) $\Gamma_7 \rightarrow \Gamma_8$ transition of $[UF_6]^-$.

power of this technique. The ability to deconvolute and assign the multitude of fine features of a single transition can provide superior insight into electronic structure and bonding in actinide coordination complexes, particularly when combined with computational studies to calculate and assign these fine structures (vide infra). For example, this approach can provide insight into the underlying mechanisms governing the shape and broadness of the fine features. As such, the extension of these studies to additional U(V) complexes with O_h symmetry was pursued to evaluate the effects of ligand type on the f—f transition signals in NIR C-term MCD.

NIR MCD Spectroscopy of $[UF_6]^-$

$[UF_6]^-$ was selected for C-term MCD investigation in the NIR region, as it is known to have larger crystal field (CF) splitting parameters, a slightly less 5f-orbital character in its frontier molecular orbitals (MOs), and less electron density in the 5f-orbitals compared to $[UCl_6]^-$.[9] Furthermore, similar high-quality NIR electronic absorption data are also available for $[UF_6]^-$ that facilitate transition assignments and provide a direct comparison to the corresponding NIR C-term MCD spectrum.[57]

An immediate difference in the 5 K, 7 T NIR MCD spectrum of $[UF_6]^-$ is the ability to observe the low energy $\Gamma_7 \rightarrow \Gamma_8$ transition from 5150 to 5850 cm^{-1}, which was too low in energy to be observed for $[UCl_6]^-$ (Fig. 2B and 2E). This is a direct result of the larger CF splitting present in $[UF_6]^-$. For this transition, the first two fine structure features can be observed from 5150 to 5350 cm^{-1}; the lower-energy signal centered at 5180 cm^{-1} contains a weak negative band and an intense positive band while the higher energy feature at 5325 cm^{-1} contains the converse. These sharp, intense features are reminiscent of the $\Gamma_7 \rightarrow \Gamma_{7'}$ transition observed in $[UCl_6]^-$. Additionally, compared to the transitions in $[UCl_6]^-$ the NIR MCD spectrum of $[UF_6]^-$ is extremely complex with numerous signals, inferring highly mixed ESs.

Moving to higher energy, the $\Gamma_7 \rightarrow \Gamma_{7'}$ transition of $[UF_6]^-$ appears from 7250 to 8050 cm^{-1}, slightly blue-shifted compared to the analogous transition in $[UCl_6]^-$ (Fig. 2D). However, the fine structure of this transition in $[UF_6]^-$ exhibits multiple differences compared to $[UCl_6]^-$. For example, the derivative feature extending from 7250 cm^{-1} to 7430 cm^{-1} with its inflection point at 7410 cm^{-1} is highly asymmetric, rather than both halves of the derivative having equal intensity, as was observed in $[UCl_6]^-$; the low-energy negative transition in $[UF_6]^-$ is over eight times as intense as the positive component. At higher energy, there is a symmetric, positive derivative signal from 7500 to 7600 cm^{-1} with an inflection point at 7540 cm^{-1}. This fine structure is significantly different than what was observed in $[UCl_6]^-$ as it is considerably weaker than the first negative feature and has a derivative shape. The final fine structure feature, from 7850 to 7970 cm^{-1}, is another slightly asymmetric negative to positive derivative signal centered at 7910 cm^{-1}. Note that the fine structure features are both less intense and more complex than for the analogous transition in $[UCl_6]^-$.

The higher energy $\Gamma_7 \rightarrow \Gamma_{8'}$ and $\Gamma_7 \rightarrow \Gamma_6$ transitions in $[UF_6]^-$ are shifted to higher energy and weak in intensity compared to the analogous transition in $[UCl_6]^-$ (see ESI, Fig. S4). For completeness, they will be briefly described. From 13500 cm^{-1} to 14250 cm^{-1} there is a weak positive to negative derivative representing the $\Gamma_7 \rightarrow \Gamma_{8'}$ transition. The $\Gamma_7 \rightarrow \Gamma_6$ transition appears from 15500 cm^{-1} to 17500 cm^{-1} as a trio of increasingly weaker positive absorption features. The extreme weakness of the vibronic coupling is an anomaly in this series and is worth considering in future studies.

Beyond halide ligands: Near-infrared MCD spectroscopy of $[U(OC_6F_5)_6]^-$, $[U(CH_2SiMe_3)_6]^-$, and $[U(NC(^tBu)(Ph))_6]^-$

While halide complexes are ideal for both experimental and theoretical (vide infra) *C*-term MCD investigations in U(V) O_h complexes, it is also of interest to expand the experimental studies to U(V) O_h systems of other ligand types. This type of study allows for the evaluation of ligand effects on the fine structure of the f—f transition in NIR *C*-term MCD. Towards this goal, the following complexes, previously reported by Hayton and co-workers were also examined through NIR *C*-term MCD spectroscopy: $[U(OC_6F_5)_6]^-$, $[U(CH_2SiMe_3)_6]^-$, and $[U(NC(^tBu)(Ph))_6]^-$.[58-60] While the resulting MCD spectra are too challenging for computational evaluation due to the significant increase in complexity of the ligand environment in these systems compared to simple halide complexes, they provide a useful experimental comparison in terms of the changes in the NIR fine features due to ligand variations beyond the simple halide complexes.

For the 5 K, 7 T MCD spectrum of $[U(OC_6F_5)_6]^-$ (Fig. 3, Top), the $\Gamma_7 \rightarrow \Gamma_{7'}$ transition from 7025 cm^{-1} to 7450 cm^{-1} contains two sharp fine structure features at 7075 cm^{-1} and 7135 cm^{-1} of an opposite sign but similar intensity. These features form a derivative shape and are followed by a series of low-intensity, higher energy signals which are positively signed. At higher energy of the spectrum, the $\Gamma_7 \rightarrow \Gamma_{8'}$ transition is observed from 10400 cm^{-1} to 11500 cm^{-1}. There are two clear fine structure peaks present at 10660 cm^{-1} and 10730 cm^{-1} that are indicative of at least two broad, negatively signed features having overlapping intensity. Also, this transition is relatively intense. This $\Gamma_7 \rightarrow \Gamma_6$ transition from 12050 cm^{-1} to 12950 cm^{-1} is the final transition observed in the NIR region, appearing almost like a standard absorption feature. With the signals being extremely close in energy, it is hard to deconvolute these individual fine structure features. The aryl oxide ligand complex's electronic transition is fairly similar to those observed in $[UCl_6]^-$ with slight perturbations. Broadly, the $\Gamma_7 \rightarrow \Gamma_{7'}$ and $\Gamma_7 \rightarrow \Gamma_{8'}$ transitions are similar in both complexes, with $[U(OC_6F_5)_6]^-$ being blue-shifted. However, the fine structural features of these transitions in $[U(OC_6F_5)_6]^-$ are closer in energy than in the previously described complexes. Specifically, in the $\Gamma_7 \rightarrow \Gamma_{7'}$ transition, there are more features present which are predominantly positively signed. Finally, the relative intensities of the transitions are more comparable in $[U(OC_6F_5)_6]^-$, while the $\Gamma_7 \rightarrow \Gamma_{7'}$ is much stronger relative to the others in $[UCl_6]^-$. With the two higher energy transitions being vibronic (this will be expanded upon in the theoretical section) it appears the ligand exchange has consequential effects on them, while the electronic transition $\Gamma_7 \rightarrow \Gamma_{7'}$ is more resilient to ligand perturbations.

$[U(CH_2SiMe_3)_6]^-$ was also probed by NIR MCD spectroscopy, as this complex is composed of pure σ-donor ligands. This provided a system to examine f—f transitions and their fine structures in NIR MCD for a U(V) complex without any ligand π-influence, unlike the three previously described systems. For the $\Gamma_7 \rightarrow \Gamma_{7'}$ transition in the 5 K, 7 T NIR MCD spectrum of $[U(CH_2Si(Me_3))_6]^-$(Fig. 3, middle), the derivative shape formed by the first two features is asymmetric with an extremely intense, sharp, negative fine structure feature at 6805 cm^{-1}. It is immediately succeeded by a weaker, positive signal at 6860 cm^{-1}. At higher energy, the $\Gamma_7 \rightarrow \Gamma_{8'}$ transition appears from 10600 cm^{-1} to 11400 cm^{-1}. This transition is both broad and relatively intense. It is comprised of multiple overlapping fine structures that are difficult to resolve, though two noticeable peaks are discernible at 10775 cm^{-1} and 11050 cm^{-1}. The final transition observed in this region is the $\Gamma_7 \rightarrow \Gamma_6$ from 12700 to 13900 cm^{-1}. It is an extremely broad negative transition that is relatively intense with the observed broadness likely resulting from multiple, overlapping fine structure features of the same sign. The $\Gamma_7 \rightarrow \Gamma_{7'}$ transition appears to be more akin to UF_6^-, though it is red-shifted in comparison to $[UCl_6]^-$ and $[U(OC_6F_5)_6]^-$ demonstrating the two clear regimes of the electronic $\Gamma_7 \rightarrow \Gamma_{7'}$ transition present in the complexes studied herein. As seen in $[U(OC_6F_5)_6]^-$ there is parity in the relative intensities of the transitions which were not observed in the halide complexes, further reflecting the sensitivity of the vibronic transitions to ligand perturbations.

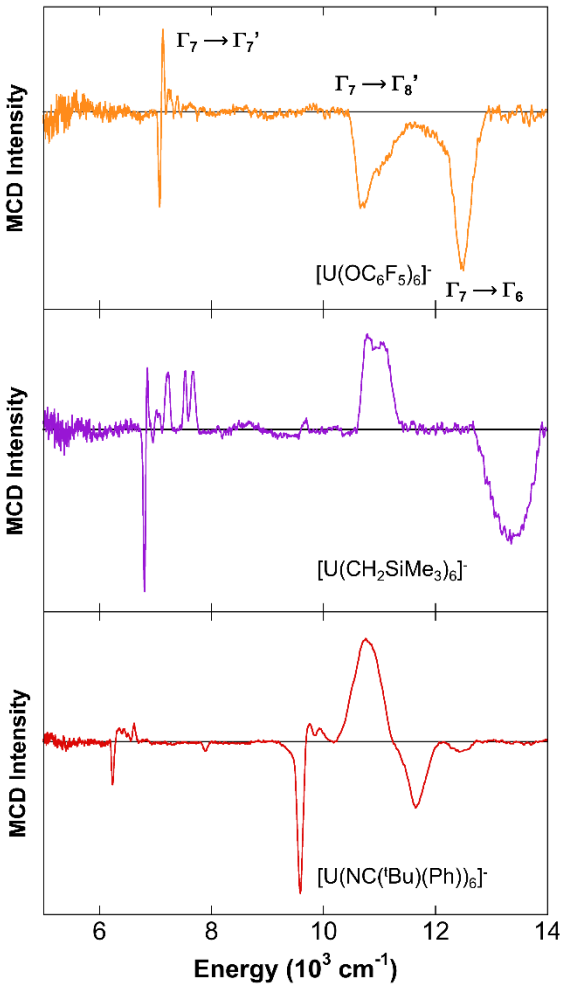

Fig. 3. The 5 K, 7 T NIR MCD spectra of top: $[U(OC_6F_5)_6]^-$, middle: $[U(CH_2SiMe_3)_6]^-$ and bottom: $[U(NC(^tBu)(Ph))_6]^-$ complexes.

The 5 K, 7 T NIR MCD spectrum of $[U(NC(^tBu)(Ph))_6]^-$ is shown in Fig. 3, bottom. This spectrum has several unique features compared to those previously reported in this study. First, the lowest energy transition starting at 6180 cm^{-1}, while sharp and derivative shaped, is very weak in intensity compared to the higher energy transitions. Furthermore, there is tremendous complexity and overlap in the higher energy

features not observed for the other complexes in this study. These fine structure features can be attributed to the complex's previously reported deviation from ideal O_h symmetry. From X-ray crystallography, this complex contains an inner sphere cation that interacts with the phenyl component of the ketamide ligands causing them to pucker. Thus, this complex demonstrates the sensitivity of the f—f transitions and fine features observable in NIR C -term MCD to not only ligand type but also geometric perturbations available from O_h symmetry.

Theoretical *C*-term MCD spectroscopy of f—f transitions of O_h U(V) complexes

The experimental NIR C-term MCD spectra of the O_h U(V) complexes described above demonstrate the detailed fine structure information that can be extracted in principle. As demonstrated in our previous C -term MCD studies of the charge transfer (CT) region of $[UCl_6]^-$,[56] this characterization method is most useful when the experimental measurements are coupled with theoretical calculations of the spectra. However, in the NIR region, these calculations are significantly more challenging than calculations of CT bands because the f—f transition intensity in a centrosymmetric environment is largely governed by vibronic coupling. Despite this challenge, calculations of the NIR MCD spectra of $[UCl_6]^-$ and $[UF_6]^-$ were pursued as representative examples of O_h U(V) complexes to evaluate simulations of these f—f transitions and to gain further insight into the origins of the transitions, fine structure features, and underlying electronic structure of these complexes.

The relevant expressions from Piepho and Schatz[61] can be used to determine the intensity of C-terms, where $\boldsymbol{x}$ is either the electric dipole ($\boldsymbol{\mu}$) or magnetic dipole ($\boldsymbol{m}$) moment operator:

$$C^x = \frac{i}{3|A|}\sum_{\alpha,\alpha',\lambda,j}\langle\Psi_{A\alpha'0}(q;Q)|\boldsymbol{L}+2\boldsymbol{S}|\Psi_{A\alpha'0}(q;Q)\rangle \cdot\left(\langle\Psi_{A\alpha0}(q;Q)|\boldsymbol{x}|\Psi_{J\lambda j}(q;Q)\rangle \times\langle\Psi_{J\lambda j}(q;Q)|\boldsymbol{x}|\Psi_{A\alpha0}(q;Q)\rangle\right) \quad (2)$$

In eqn (2), $\Psi(q;Q)$ represents the wavefunction depending on electronic (q) and nuclear (Q) degrees of freedom: α and λ are components of the GS (A) and the ES (J), subscript '0' indicates that the initial state (GS) A is in the vibrational zero-point level, while the index 'j' characterizes a vibrational sub-state of the excited state (ES) J. Underlying the separation of the vibrational and electronic components of the wavefunctions is the Born-Oppenheimer (BO) approximation, where

$$|\Psi_{J\lambda j}(q;Q)\rangle = |\psi_{J\lambda}(q;Q)\rangle|\chi_{Jj}(Q)\rangle \quad (3)$$

Here, $\psi_{J\lambda}(q;Q)$ and $\chi_{Jj}(Q)$ represent the adiabatic electronic and the nuclear vibrational wavefunctions, respectively.

The f—f transitions are magnetic-dipole allowed, while at the same time the vibronic contributions to the MCD via the magnetic transition-dipole moments (TDMs) can be considered negligible compared to the vibronic contributions to the electric TDMs. Therefore, the intensities of the purely electronic transitions were calculated from the magnetic transition-dipole moments according to Piepho and Schatz.[61]

$$C^m = \frac{i}{3|A|}\sum_{\alpha,\alpha',\lambda}\langle\psi_{A\alpha'}|\boldsymbol{L}+2\boldsymbol{S}|\psi_{A\alpha'}\rangle \cdot\left(\langle\psi_{A\alpha}|\boldsymbol{m}|\psi_{J\lambda}\rangle\times\langle\psi_{J\lambda}|\boldsymbol{m}|\psi_{A\alpha}\rangle\right) \quad (4)$$

The Herzberg-Teller (HT) vibronic coupling model was used to treat the contributions to the MCD from the electric transition-dipole moments. Accordingly, a Taylor series expansion of TDM in terms of the normal modes was set up:

$$\langle\chi_{A0}(Q)|\boldsymbol{\mu}^e_{A\alpha,J\lambda}(Q)|\chi_{Jj}(Q)\rangle = \boldsymbol{\mu}^e_{A\alpha,J\lambda}(Q_0)\langle\chi_{A0}(Q)|\chi_{Jj}(Q)\rangle + \sum_{p=1}^{M}\langle\chi_{A0}(Q)|Q_p|\chi_{Jj}(Q)\rangle\left(\frac{\partial\boldsymbol{\mu}^e_{A\alpha,J\lambda}(Q)}{\partial Q_p}\right)\Big|_{Q_0}+\cdots \quad (5)$$

In the previous equation, the electric transition-dipole moment between the electronic states is $\boldsymbol{\mu}^e_{A\alpha,J\lambda}(Q) = \langle\psi_{A\alpha}(q;Q)|\boldsymbol{\mu}|\psi_{J\lambda}(q;Q)\rangle$, Q_0 is the equilibrium position of the M nuclei, and Q_p is one of the $M = 3N-6$ vibrational modes for a non-linear molecule.

The TDM derivatives in eqn (5) were calculated via a sum-over-state (SOS) perturbation theory approach:[62, 63]

$$\frac{\partial\boldsymbol{\mu}^e_{A\alpha,J\lambda}(Q)}{\partial Q_p} = \sum_{Kk\neq J\lambda}\langle\psi^0_{Kk}|\boldsymbol{\mu}^e|\psi^0_{J\lambda}\rangle\frac{\langle\psi^0_{A\alpha}|\partial H/\partial Q_p|\psi^0_{Kk}\rangle}{E^0_{A\alpha}-E^0_{Kk}} + \sum_{Kk\neq A\alpha}\langle\psi^0_{A\alpha}|\boldsymbol{\mu}^e|\psi^0_{Kk}\rangle\frac{\langle\psi^0_{Kk}|\partial H/\partial Q_p|\psi^0_{J\lambda}\rangle}{E^0_{J\lambda}-E^0_{Kk}} \quad (6)$$

Here, superscript '0' indicates a state calculated at $Q = Q_0$; k represents the component of electronic state K used in SOS; and H is the molecular Hamiltonian. The Hamiltonian derivatives $\langle\psi^0_{Kk}|\partial H/\partial Q_p|\psi^0_{J\lambda}\rangle$, appearing in eqn (6), are calculated numerically by a central finite difference approach in the form of $\partial\langle\psi^0_{Kk}|H|\psi^0_{J\lambda}\rangle/\partial Q_p$, as suggested by Orlandi and others,[64] utilizing a "floating" atomic orbital (FAO) basis that moves with the nuclei along Q_p, while the wavefunction parameters remain those of the equilibrium structure. Matrix elements $\langle\psi^0_{Kk}|\boldsymbol{\mu}^e|\psi^0_{J\lambda}\rangle$ and $\langle\psi^0_{A\alpha}|\boldsymbol{\mu}^e|\psi^0_{J\lambda}\rangle$ facilitate intensity "borrowing" from state ψ^0_{Kk} that has the opposite parity of $\psi^0_{A\alpha}$ and $\psi^0_{J\lambda}$. The vibronic TDMs among the spin-orbit (SO)-coupled states are obtained from *a posteriori* transformation of spin-free (SF) $\boldsymbol{\mu}^e_{A\alpha,J\lambda}$ with the coefficients that mix different spin-states via state interaction**.** This setup was previously tested in calculations of vibronic f—f absorption spectra and was found to perform reasonably well.

The matrix element $\langle\chi_{A0}(Q)|Q_p|\chi_{Jj}(Q)\rangle$ in eqn (5) are commonly calculated by expanding the vibrational normal modes of one of the states in terms of the normal modes of the other state. Here, we are dealing with the electronic transitions between LF states involving weakly (anti-)bonding metal 5f

Complex	RAS-SO ΔE$_{elec.}$[b]	RAS-SO ΔE$_{vib.}$[b]	RAS-SO C[c]	PT2-SO ΔE$_{elec.}$	PT2-SO ΔE$_{vib.}$[b]	PT2-SO C[c]
[UCl$_6$]$^-$	6988		-0.476E-04	7048		-0.501E-04
			0.156E-03		7130	0.270E-04
			-0.208E-03		7162	0.100E-06
			-0.190E-03		7349	-0.954E-05
[UF$_6$]$^-$	7279		-0.524E-04	7506		-0.510E-04
		7413	0.639E-04		7640	0.399E-04
		7453	0.575E-04		7680	-0.160E-05
		7795	0.139E-04		8022	-0.248E-04

[a]H-T expansion of the zeroth-order wavefunction uses the experimental geometry

[b]Electronic (ΔE$_{elec.}$) and vibronic (ΔE$_{vib.}$) energies are in photon wavenumbers (cm^{-1})

[c]MCD terms are in Debye

Table 1 RAS-SO vs. PT2-SO Electronic and Vibronic Absorption Energies corresponding to $\Gamma_7 \rightarrow \Gamma_{7'}$ Excitation[a] and MCD C-terms for UX_6^- (X = F, Cl) complexes.

orbitals. Therefore, we assumed the equilibrium structures of the GS and ESs are essentially the same and the vibrational wavefunctions $|\chi_{A0}\rangle$ and $|\chi_{Jj}\rangle$ are approximated as products of the same harmonic vibrational modes: $|\xi_1^a \xi_2^b \dots \xi_p^c \dots \xi_M^x\rangle$and $|\xi_1^k \xi_2^l \dots \xi_p^m \dots \xi_M^y\rangle$. From a recursive relation,[66] the value of the integral $\langle \chi_{A0}(Q)|Q_p|\chi_{Jj}(Q)\rangle$ is non-zero if $\nu_p = \pm 1$, with a value of $(8\pi^2 c\nu_p/h(\nu_p+1))^{-1/2}$ for $\nu_p = +1$, and $(8\pi^2 c\nu_p/h\nu_p)^{-1/2}$ for $\nu_p = -1$. At 5 K, only $\nu_p = +1$ transitions are observed because excited vibrational levels are not populated. Vibronic transitions occur at an energy of $\Delta E_{A\alpha,J\lambda} = \Delta E^e_{A\alpha,J\lambda} + h\nu_p$, where $\Delta E^e_{A\alpha,J\lambda}$ is the energy difference between the electronic states involved in the transition, which is accompanied by excitation of the p-th vibrational mode.

Ab initio wavefunction calculations were performed using the Restricted Active Space (RAS) self-consistent field method and a developers' version of the [Open]Molcas software.[65,66] For full computational details see section S2 in the ESI. In the following, RAS-SO indicates RAS wavefunction calculations including SO coupling. Calculations labels as PT2-SO also include corrections to the state energies from the dynamic electron correlation via 2nd order perturbation theory.

Calculated NIR *C*-term MCD spectra of $[UCl_6]^-$ and $[UF_6]^-$

Employing the theoretical methods described above, NIR f—f transitions in *C*-term MCD spectra can be simulated. The calculations decipher the origin of the spectral features of these complexes, particularly the importance of the sensitivity of the fine structure features (shape and sign) to ligand identity.

In the SF picture, the GS of UX_6^- (X = F, Cl) is orbitally non-degenerate $^2A_{2u}$, while the lowest-energy LF ESs are the orbitally triply-degenerate $^2T_{2u}$ and $^2T_{1u}$.[61,64] In the O_h double-group, the $^2A_{2u}$ transforms as Γ_7, the $^2T_{2u}$ splits into Γ_8 and $\Gamma_{7'}$, and $^2T_{1u}$ splits into an $\Gamma_{8'}$ and Γ_6 under the first-order SO coupling, and the same symmetry species mix further under the SO coupling such that the GS (Γ_7 = 60%$^2A_{2u}$ + 40%$^2T_{2u}$) acquires some orbital degeneracy through mixing with spatially degenerate excited spin-states.[57,67] The attained spatial degeneracy of the GS gives rise to a significant contribution of the *C*-terms to the MCD spectrum at 5 K. Additionally, along with the ligand identity, it is interesting to observe the change in fine structure features and with geometric perturbations and the deviations from O_h point group symmetry, and choice of theoretical methods. Experimental structures were used for the H-T expansion and vibrational normal modes obtained from optimized O_h structures were mapped onto experimental structures (for details see section 1.4.3 in the ESI). The corresponding LF spectra for UX_6^- (X = F, Cl) complexes are presented in Fig. S5 and S6 in the ESI and show good agreement with the experiment. Note, as mentioned above, the first LF transition ($\Gamma_7 \rightarrow \Gamma_8$) is out of range of the experimental LF MCD spectra for UCl_6^-. Therefore, we begin our discussion with the $\Gamma_7 \rightarrow \Gamma_{7'}$ LF transition, which is the lowest energy transition observable transition in both complexes that has been calculated to have significant intensity not just from vibronic coupling but also from the purely electronic magnetic-dipole transition.

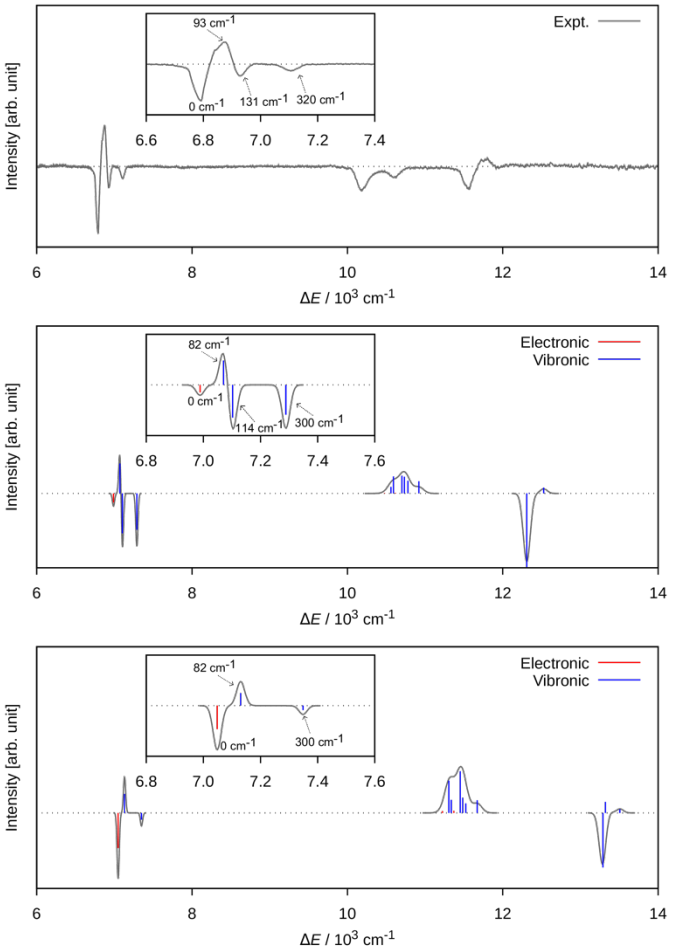

Fig. 4. The f—f LF MCD spectra of UCl_6^-: Top: the experimental LF spectrum. Middle: LF MCD spectra (5 K) calculated with RAS-SO using experimental structure for H-T expansion. Bottom: LF MCD spectra (5 K) calculated with PT2-SO using experimental structure for H-T expansion. Calculated $\Gamma_7 \rightarrow \Gamma_{7'}$ transitions were Gaussian-broadened with FWHM = 25 cm^{-1}, $\Gamma_7 \rightarrow \Gamma_8$ transitions were Gaussian-broadened with FWHM = 200 cm^{-1}, and $\Gamma_7 \rightarrow \Gamma_6$ transitions were Gaussian-broadened with FWHM = 150 cm^{-1}. The sharp and intense $\Gamma_7 \rightarrow \Gamma_{7'}$ LF MCD peaks are shown in the inset for clarity. The contributions of electronic and vibronic transitions are denoted with different colors in the underlying "stick spectra".

$[UCl_6]^-$. For the $\Gamma_7 \rightarrow \Gamma_{7'}$ LF transition in $[UCl_6]^-$, the experimental MCD spectrum contains three negative and one positive fine structure features. The lowest-energy sharp negative feature is calculated to be the magnetic-dipole allowed electronic transition, while the higher energy three consecutive weaker features are the vibronic transitions. The calculated RAS-SO and PT2-SO simulated MCD spectra for this LF transition are blue-shifted by ~250 cm^{-1} and 300 cm^{-1}, respectively, which is well within the error bars of this type of calculation, and fall within the range of ~6950 - 7350 cm^{-1}. The calculated broadened spectra along with the experimental spectrum are

presented in Fig. 4. Numerical data for the $\Gamma_7 \rightarrow \Gamma_{7'}$ LF transition are collected in Table 1. In the experimental spectrum, there is a shoulder to the first vibronic feature at 23 cm^{-1} which does not correspond to any vibrational frequency, therefore, it was not reproduced in the calculations. Hecht et al. showed evidence that this feature could be due to coupling with an unassigned low energy mode,[68] while Ohwada attributed a similar feature to a rotational or translational lattice vibrational mode.[69] The sign, shape, and energy for all the fine structure features are well simulated with RAS-SO. However, with RAS-SO, the magnetic-dipole allowed transitions were less intense than in the experiment, which is reflected in the relative intensity between electronic and vibronic transitions. The relative intensity is better reproduced with PT2-SO, although the third fine structure feature in this band is very weak and therefore not visible in the PT2-SO spectrum. The first derivative-like feature is created by two consecutive electronic and vibronic (82 cm^{-1}) transitions. It is nicely reproduced with both RAS-SO and PT2-SO, but not when the O_h structure was used for the zeroth-order wavefunction calculation in the H-T expansion (see Fig. S7 in the ESI). The sign of the other vibronic fine structure feature is also opposite to the experiment when O_h structures were used (see Fig. S7 in the ESI). Overall, therefore, the LF MCD spectra are quite sensitive to approximations made in the calculations, including the choice of structure for the HT expansion. This indicates that future vibronic MCD calculations need to be improved and treat Duschinsky rotations and related effects explicitly.

Likewise, the higher energy $\Gamma_7 \rightarrow \Gamma_{8'}$ transition turns out to be difficult to simulate. The RAS-SO simulated MCD spectrum for this particular LF transition is blue-shifted by ~400 cm^{-1} whereas the PT2-SO simulated spectrum for the same is blue-shifted by ~1100 cm^{-1}. Unfortunately, the sign of the band is opposite in the experiment vs. the calculations. We tentatively attribute this to the fact that the ES is orbitally degenerate in O_h symmetry and may undergo a distortion that we are presently not able to model.

Going to the highest energy $\Gamma_7 \rightarrow \Gamma_6$ transition, the RAS-SO, and PT2-SO MCD features match reasonably well with the experiment. In the simulated MCD spectra using the experimental geometry. Both the RAS-SO and the PT2-SO spectra are blue-shifted by ~750 cm^{-1} and ~1700 cm^{-1}, respectively, relative to the experiment. However, as pointed out already, such deviations are not untypical in calculations of electronic excitation energies with the methods used. The simulated spectra capture the derivative shape of the band qualitatively.

$[UF_6]^-$. Due to the interest in the $\Gamma_7 \rightarrow \Gamma_{7'}$ LF transition, as it is the only one with significant magnetic dipole character, the MCD spectrum for this transition was calculated for UF_6^- as well to evaluate the different LF of fluoride. The simulated spectra along with the experimental spectrum are shown in Fig. 5. Numerical data for this transition are collected in Table 1. The calculated RAS-SO spectrum is slightly red-shifted by ~100 cm^{-1} while the PT2-SO spectrum is slightly blue-shifted by ~120 cm^{-1}, relative to the experiment. Both RAS-SO and PT2-SO predict the first negative peak is due to the magnetic TDM of the electronic transition while the higher energy peaks are vibronic. Similar to $[UCl_6]^-$ there is a feature at 33 cm^{-1} that does not correspond to any vibrational frequency, therefore, it is not produced in the calculations. Similar explanations[68,69] as for the 23 cm^{-1} feature in $[UCl_6]^-$ apply here as well. The comparison of the calculated and measured spectra likewise shows that fine structure details of the MCD can be assigned with the help of the calculations, but in some cases, even the signs of the vibronic peaks are challenging to obtain. For the MCD spectra simulated using O_h structure see Fig. S8 in the ESI.

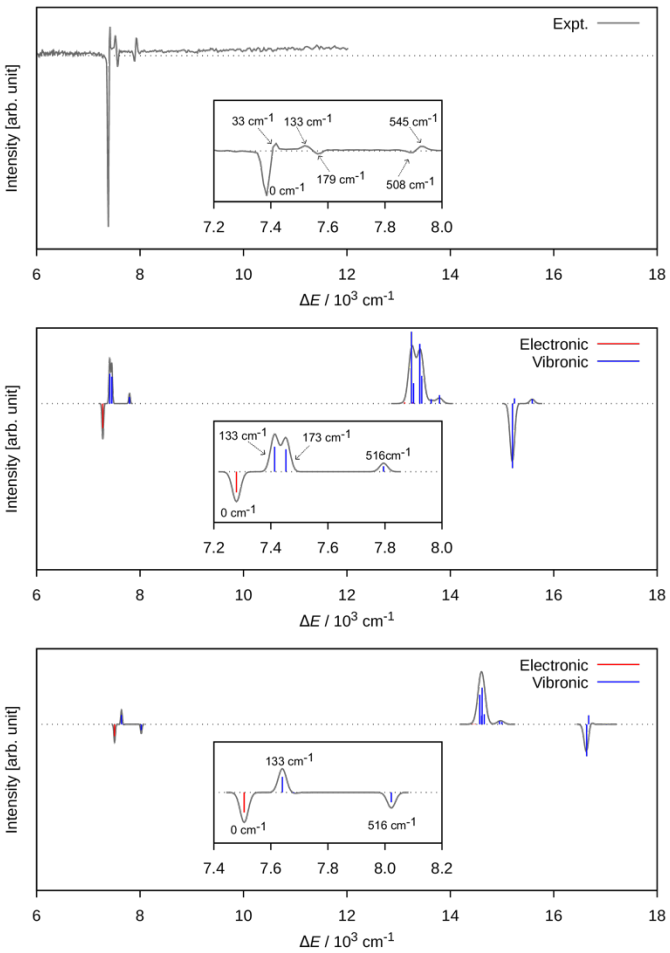

Fig. 5. The f—f LF MCD spectra of $[UF_6]^-$: Top: the experimental LF spectrum. Middle: LF MCD spectra (5 K) calculated with RAS-SO using experimental structure for H-T expansion. Bottom: LF MCD spectra (5 K) calculated with PT2-SO using experimental structure for H-T expansion. Calculated $\Gamma_7 \rightarrow \Gamma_{7'}$ transitions were Gaussian-broadened with FWHM = 25 cm-1, $\Gamma_7 \rightarrow \Gamma_8$ transitions were Gaussian-broadened with FWHM = 200 cm^{-1}, and $\Gamma_7 \rightarrow \Gamma_6$ transitions were Gaussian-broadened with FWHM = 150 cm^{-1}. The sharp and intense $\Gamma_7 \rightarrow \Gamma_{7'}$ LF MCD peaks are shown in the inset for clarity. The contributions of electronic and vibronic transitions are denoted with different colors in the underlying "stick spectra".

Conclusion

Insight into the electronic structure of actinide complexes is critical to defining the roles of d- and f-orbitals in bonding and reactivity. Towards this goal, we have focused on the experimental and theoretical development of low-temperature *C*-term MCD spectroscopy to probe f—f transitions in the NIR

region of U(V) O_h complexes, which have been of longstanding interest for probing electronic structure, bonding, and covalency in 5f systems. *C* -term MCD spectra of the f—f transitions in $[UCl_6]^-$ and $[UF_6]^-$ (and additional non-halide O_h complexes) demonstrate the high-resolution low energy transitions that can be obtained with these methods, including additional fine structure facilitated by the signed nature of the transitions. In addition, theoretical methods were developed to calculate the experimentally observed spectra of the halide complexes from first principles, providing further insight into the origins of these transitions and their associated fine features. Overall, the spectra and simulations reported herein provide an important platform for the application of MCD spectroscopy to this widely studied class of U(V) complexes and identify areas for continued theoretical development.

Conflicts of interest

The authors declare no conflicts of interest.

Acknowledgements

M.L.N acknowledges support for this work from the U.S. Department of Energy, Office of Science, Early Career Research Program under Award DE-SC0016002. J.A. acknowledges support from the U.S. Department of Energy, Office of Science, Basic Energy Sciences, Heavy Element Chemistry, grant DE-SC0001136. S.G.M. was supported by the Director, Office of Science, Office of Basic Energy Sciences, Division of Chemical Sciences, Geosciences, and Biosciences Heavy Element Chemistry Program of the U.S. Department of Energy at LBNL under Contract No. DE-AC02-05CH11231. S.A.K. anckonweldges support from the U.S. Department of Energy, Office of Science, Office of Basic Energy Sciences, Heavy Element Chemistry program (2020LANLE372). LANL is an affirmative action/equal opportunity employer managed by Triad National Security, LLC, for the National Nuclear Security Administration of the U.S. DOE. We thank the Center for Computational Research (CCR) at the University of Buffalo for providing computational resources.

References

1. Q. Sun, B. Aguila, J. Perman, A. S. Ivanov, V. S. Bryantsev, L. D. Earl, C. W. Abney, L. Wojtas and S. Ma*, Nat. Commun*., 2018, **9**, 1644.
2. I. Castro-Rodríguez, H. Nakai and K. Meyer, *Angew. Chem. Int. Ed.*, 2006, **45**, 2389-2392.
3. S. M. Mansell, N. Kaltsoyannis and P. L. Arnold*, J. Am. Chem. Soc.,* 2011, **133**, 9036-9051.
4. V. Mougel, C. Camp, J. Pécaut, C. Copéret, L. Maron, C. E. Kefalidis and M. Mazzanti*, Angew. Chem. Int. Ed.*, 2012, **51**, 12280-12284.
5. J. J. Kiernicki, M. G. Ferrier, J. S. Lezama Pacheco, H. S. La Pierre, B. W. Stein, M. Zeller, S. A. Kozimor, and S. C. Bart, *J. Am. Chem. Soc.,* 2016, **138**, 13941–13951.
6. V. A. Volkovich, I. May, T. R. Griffiths, J. M. Charnock, A. I. Bhatt, and B. Lewin, *J. Nucl. Matter.,* 2005, **344**, 100-103.
7. W. B. Lewis, H. G. Hecht, and M. P. Eastman, *Inorg. Chem.*, 1973, **12**, 1634-1639.
8. C. R. Graves, P. Yang, S. A. Kozimor, A. E. Vaughn, D. L. Clark, S. D. Conradson, E. J. Schelter, B. L. Scott, J. D. Thompson, P. J. Hay, D. E. Morris and J. L. Kiplinger, *J. Am. Chem. Soc*., 2008, **130**, 5272-5285.
9. W. W. Lukens, N. M. Edelstein, N. Magnani, T. W. Hayton, S. Fortier and L. A. Seaman, *J. Am. Chem. Soc.*, 2013, **135**, 10742-10754.
10. J. J. Kiernicki, C. J. Tatebe, M. Zeller and S. C. Bart, *Inorg. Chem*., 2018, **57**, 1870-1879.
11. F. Jollet, T. Petit, S. Gota, N. Thromat, M. Gautier-Soyer and A. Pasturel, *J. Phys.: Cond. Mat.,* 1997, **9**, 9393-9401.
12. S. W. Yu, J. G. Tobin, J. C. Crowhurst, S. Sharma, J. K. Dewhurst, P. Olalde-Velasco, W. L. Yang and W. J. Siekhaus, *Phys. Rev. B*, 2011, **83**, 165102.
13. S. M. Butorin, K. O. Kvashnina, D. Prieur, M. Rivenet and P. M. Martin, *Chem. Commun*., 2017, **53**, 115-118.
14. J. Su, E. R. Batista, K. S. Boland, S. E. Bone, J. A. Bradley, S. K. Cary, D. L. Clark, S. D. Conradson, A. S. Ditter, N. Kaltsoyannis, J. M. Keith, A. Kerridge, S. A. Kozimor, M. W. Löble, R. L. Martin, S. G. Minasian, V. Mocko, H. S. LaPierre, G. T. Seidler, D. K. Shuh, M. P. Wilkerson, L. E. Wolfsberg, and P. Yang, *J. Am. Chem. Soc*., 2018, **140**, 17977-17984.
15. S. G. Minasian, J. M. Keithm, E. R. Batista, K. S. Boland, D. L. Clark, S. D. Conradson, S. A Kozimor, R. L. Martin, D. E. Schwarz, D. K. Shuh, G. L. Wagner, M. P. Wilkerson, L. E. Wolfsberg, and P. Yang*, J. Am. Chem. Soc.*, 2012, **134**, 5586-5597.
16. T. Vitova, K. O. Kvashnina, G. Nocton, G. Sukharina, M. A. Denecke, S. M. Butorin, M. Mazzanti, R. Caciuffo, A. Soldatov, T. Behrends, and H. Geckeis, *Phys. Rev. B*, 2010, **82**, 235118.
17. S. M. Butorin, K. O. Kvashnina, D. Prieur, M. Rivenet, and P. M. Martin, *Chem. Commun.,* 2017, **53**, 115-118.
18. M. A. Denecke, *Dalton Trans.*, 2015, **44**, 2606-2612.
19. S. M. Butorin, K. O. Kvashnina, J. R. Vegelius, D. Meyer, and D. K. Shuh, *Proc. Natl. Acad. Sci. U.S.A.*, 2016, **113**, 8093-8097.
20. D. Prieur, F. Lebreton, P. M. Martin, M. Caisso, R. Butzbach, J. Somers, and T.Delahaye, *J. Solid State Chem.*, 2015, **230**, 8-13
21. C. G. Gianopoulos, V. V. Zhurov, S. G. Minasian, E. R. Batista, C. Jelsch, and A. A. Pinkerton, *Inorg. Chem.*, 2017, **56**, 1775-1778.
22. A.-C. Schmidt, F. W. Heinemann, W. W. Lukens and K. Meyer, *J. Am. Chem. Soc.,* 2014, **136**, 11980-11993.
23. H. S. La Pierre, A. Scheurer, F. W. Heinemann, W. Hieringer and K. Meyer*, Angew. Chem. Int. Ed.*, 2014, **53**, 7158-7162.
24. D. M. King, P. A. Cleaves, A. J. Wooles, B. M. Gardner, N. F. Chilton, F. Tuna, W. Lewis, E. J. L. McInnes and S. T. Liddle, *Nat. Commun.*, 2016, **7**, 13773.
25. A. Formanuik, A.-M. Ariciu, F. Ortu, R. Beekmeyer, A. Kerridge, F. Tuna, E. J. L. McInnes and D. P. Mills, *Nat. Chem.,* 2017*,* **9**, 578–583.

26. K. Herasymchuk, L. Chiang, C. E. Hayes, M. L. Brown, J. S. Ovens, B. O. Patrick, D. B. Leznoff, and T. Storr, *Dalton Trans.*, 2016, **45**, 12576-12586.
27. A. J. Lewis, E. Nakamaru-Ogiso, J. M. Kikkawa, P. J. Carroll, and E. J. Schelter, *Chem. Commun.,* 2012, **48**, 4977-4979.
28. H. Nakai, X. Hu, L. N. Zakharov, A. L. Rheingold, and K. Meyer, *Inorg. Chem.,* 2004, **43**, 855–857.
29. M. M. Abraham and L. A. Boatner, *J. Chem. Phys*., 1984, **81**, 2528-2534.
30. L. K. Aminov, I. N. Kurkin, and B. Z. Malkin, *Phys. Solid State, 2*013, **55**, 1343-1363.
31. C. R. Graves, A. E. Vaughn, E. J. Schelter, B. L. Scott, J. D. Thompson, D. E. Morris and J. L. Kiplinger, *Inorg. Chem*., 2008, **47**, 11879-11891.
32. D. E. Smiles, G. Wu, P. Hrobárik and T. W. Hayton, *J. Am. Chem. Soc*., 2016, **138**, 814-825.
33. J. J. Kiernicki, M. G. Ferrier, J. S. Lezama Pacheco, H. S. La Pierre, B. W. Stein, M. Zeller, S. A. Kozimor and S. C. Bart, *J. Am. Chem. Soc*., 2016, **138**, 13941-13951.
34. H. Ramanantoanina and M. Gruden, *Int. J. Quantum Chem.*, 2020, **120**, 26081.
35. S. Duhović, J. V. Oria, S. O. Odoh, G. Schreckenbach, E. R. Batista, and P. L. Diaconescu, *Organometallics,* 2013, **32**, 6012–602.
36. S. G. Minasian, J. M. Keith, E. R. Batista, K. S. Boland, D. L. Clark, S. A. Kozimor, R. L. Martin, D. K. Shuh, and T. Tyliszczak, *Chem. Sci.*, 2014, **5**, 351-359.
37. S. Knecht, H. J. Aa. Jensen and T. Saue, *Nat. Chem.*, 2019, **11**, 40–44.
38. G. Liu, C. Zhang, S. M. Ciborowski, A. Asthana, L. Cheng, and K. H. Bowen, *J. Phys. Chem. A,* 2020, **124**, 6486–6492.
39. L. Zhang, B. Fang, G. Zi, W. Ding, and M. D. Walter, *Organometallics,* 2017, **36**, 898–910.
40. B. E. Bursten, L. F.Rhodes, and R. J. Strittmatter, *J. Am. Chem. Soc.,* 1989, **111**, 2756-2758.
41. J. Su, P. D. Dau, H.-T. Liu, D.-L. Huang, F. Wei, W. H. E. Schwarz, J. Li, and L.-S. Wang, *J. Chem. Phys.*, 2015, **142**, 134308.
42. N. Edelstein, D. Brown, and B. Whittaker, *Inorg. Chem.*, 1974, **13**, 563-567.
43. R. Beekmeyer, and A. Kerridge, *Inorganics,* 2015, **3**, 482-499.
44. N. M. Edelstein, and W. W. Lukens, *J. Phys. Chem. A*, 2020, **124**, 4253-4262.
45. G. Ganguly, D.-C. Sergentu, and J. Autschbach, *Chem. Eur. J.*, 2020, **26**, 1776-1788.
46. D.-C. Sergentu, T. J. Duignan, and J. Autschbach, *J. Phys. Chem. Lett.*, 2018, **9**, 5583-5591.
47. D.-C. Sergentu, F. Gendron, and J. Autschbach, *Chem. Sci.*, 2018, **9**, 6292-6306.
48. B. R. Sook, D. R. Block, S. Sumithran, G. E. Montañez, K. R. Rodgers, J. H. Dawson, Z. Eichenbaum and D. W. Dixon, *Biochem*., 2008, **47**, 2678-2688.
49. S. L. Daifuku, M. H. Al-Afyouni, B. E. R. Snyder, J. L. Kneebone and M. L. Neidig*, J. Am. Chem. Soc*., 2014, **136**, 9132-9143.
50. S. Hong, K. D. Sutherlin, J. Park, E. Kwon, M. A. Siegler, E. I. Solomon and W. Nam, *Nat. Commun.,* 2014, **5**, 5440.
51. H.-D. Amberger, H. Reddmann and N. M. Edelstein, *Inorg. Chim. Acta*, 1987, **139**, 339.
52. S. De Houwer, K. Servaes and C. Görller-Walrand, *Phys. Chem. Chem. Phys*., 2003, **5**, 1164-1168.
53. J. T. Coutinho, M. Perfetti, J. J. Baldoví, M. A. Antunes, P. P. Hallmen, H. Bamberger, I. Crassee, M. Orlita, M. Almeida, J. van Slageren and L. C. J. Pereira*, Chem. Eur. J.*, 2019, **25**, 1758-1766.
54. N. J. Wolford, D.-C. Sergentu, W. W. Brennessel, J. Autschbach and M. L. Neidig, *Angew. Chem. Int. Ed*., 2019, **58**, 10266-10270.
55. N. J. Wolford, X. Yu, S. C. Bart, J. Autschbach and M. L. Neidig, *Dalton Trans.,* 2020, **49**, 14401-14410.
56. F. Gendron, V. E. Fleischauer, T. J. Duignan, B. L. Scott, M. W. Löble, S. K. Cary, S. A. Kozimor, H. Bolvin, M. L. Neidig and J. Autschbach, *Phys. Chem. Chem. Phys*., 2017, **19**, 17300-17313.
57. M. J. Reisfeld and G. A. Crosby, *Inorg. Chem*., 1965, **4**, 65-70.
58. S. Fortier, G. Wu and T. W. Hayton*, Inorg. Chem.,* 2009, **48**, 3000-3011.
59. S. Fortier, J. R. Walensky, G. Wu and T. W. Hayton, *J. Am. Chem. Soc.*, 2011, **133**, 11732-11743.
60. L. A. Seaman, G. Wu, N. Edelstein, W. W. Lukens, N. Magnani and T. W. Hayton, *J. Am. Chem. Soc.*, 2012, **134**, 4931-4940.
61. S. B. Piepho and P. N. Schatz, *Group Theory in Spectroscopy with Applications to Magnetic Circular Dichroism*, 1983, John Wiley & Sons; New York.
62. Y. N. Heit, F. Gendron and J. Autschbach, *J. Phys. Chem. Let*., 2018, **9**, 887-894.
63. G. Ganguly, H. D. Ludowieg and J. Autschbach, *J. Chem. Theory Comput.*, 2020, **16**, 5189-5202.
64. G. Orlandi and W. Siebrand, *J. Chem. Phys.,* 1973, **58**, 4513-4523.
65. F. Aquilante, J. Autschbach, A. Baiardi, S. Battaglia, V. A. Borin, L. F. Chibotaru, I. Conti, L. D. Vico, M. Delcey, I. F. Galván, N. Ferré, L. Freitag, M. Garavelli, X. Gong, S. Knecht, E. D. Larsson, R. Lindh, M. Lundberg, P. Å. Malmqvist, A. Nenov, J. Norell, M. Odelius, M. Olivucci, T. B. Pedersen, L. Pedraza-González, Q. M. Phung, K. Pierloot, M. Reiher, I. Schapiro, J. Segarra-Martí, F. Segatta, L. Seijo, S. Sen, D.-C. Sergentu, C. J. Stein, L. Ungur, M. Vacher, A. Valentini and V. Veryazov, *J. Chem. Phys.*, 2020, **152**, 214117.
66. I. Fdez. Galván, M. Vacher, A. Alavi, C. Angeli, F. Aquilante, J. Autschbach, J. J. Bao, S. I. Bokarev, N. A. Bogdanov, R. K. Carlson, L. F. Chibotaru, J. Creutzberg, N. Dattani, M. G. Delcey, S. S. Dong, A. Dreuw, L. Freitag, L. M. Frutos, L. Gagliardi, F. Gendron, A. Giussani, L. González, G. Grell, M. Guo, C. E. Hoyer, M. Johansson, S. Keller, S. Knecht, G. Kovačević, E. Källman, G. Li Manni, M. Lundberg, Y. Ma, S. Mai, J. P. Malhado, P. Å. Malmqvist, P. Marquetand, S. A. Mewes, J. Norell, M. Olivucci, M. Oppel, Q. M. Phung, K. Pierloot, F. Plasser, M. Reiher, A. M. Sand, I. Schapiro, P. Sharma, C. J. Stein, L. K. Sørensen, D. G. Truhlar, M. Ugandi, L. Ungur, A. Valentini, S. Vancoillie, V. Veryazov, O. Weser, T. A. Wesołowski, P.-O. Widmark, S.

Wouters, A. Zech, J. P. Zobel and R. Lindh, *J. Chem. Theory Comput*., 2019, **15**, 5925-5964.

67. S. G. Minasian, J. M. Keith, E. R. Batista, K. S. Boland, D. L. Clark, S. D. Conradson, S. A. Kozimor, R. L. Martin, D. E. Schwarz, D. K. Shuh, G. L. Wagner, M. P. Wilkerson, L. E. Wolfsberg and P. Yang, *J. Am. Chem. Soc.*, 2012, **134**, 5586-5597.
68. H. G. Hecht, J. G. Malm, J. Foropoulos and W. T. Carnall, *J. Chem. Phys.*, 1986, **84**, 3653-3662.
69. K. Ohwada, *Applied Spect*., 1990, **44**, 844-848.